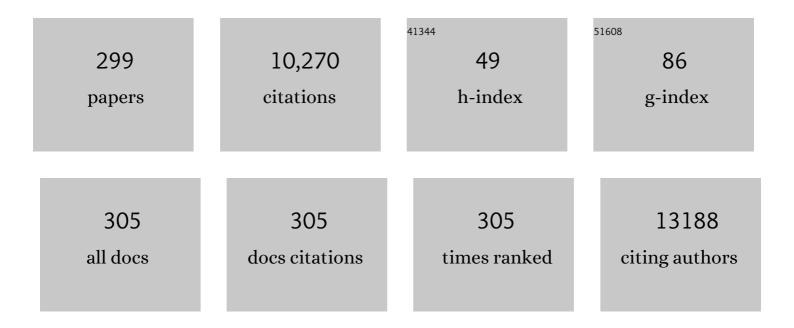
Igor Polikarpov

List of Publications by Year in descending order

Source: https://exaly.com/author-pdf/2153381/publications.pdf Version: 2024-02-01



ICOP POLIKAPPOV

#	Article	IF	CITATIONS
1	Bovine β-lactoglobulin at 1.8 à resolution — still an enigmatic lipocalin. Structure, 1997, 5, 481-495.	3.3	674
2	Average protein density is a molecular-weight-dependent function. Protein Science, 2009, 13, 2825-2828.	7.6	552
3	Determination of the molecular weight of proteins in solution from a single small-angle X-ray scattering measurement on a relative scale. Journal of Applied Crystallography, 2010, 43, 101-109.	4.5	389
4	Chemical and morphological characterization of sugarcane bagasse submitted to a delignification process for enhanced enzymatic digestibility. Biotechnology for Biofuels, 2011, 4, 54.	6.2	382
5	Crystal structure of the extracellular region of human tissue factor. Nature, 1994, 370, 662-666.	27.8	230
6	Medium Chain Fatty Acids Are Selective Peroxisome Proliferator Activated Receptor (PPAR) Î ³ Activators and Pan-PPAR Partial Agonists. PLoS ONE, 2012, 7, e36297.	2.5	165
7	Enzymatic hydrolysis of pretreated sugar cane bagasse using Penicillium funiculosum and Trichoderma harzianum cellulases. Process Biochemistry, 2011, 46, 1196-1201.	3.7	148
8	Substrate binding is required for assembly of the active conformation of the catalytic site in Ntn amidotransferases: evidence from the 1.8 å crystal structure of the glutaminase domain of glucosamine 6-phosphate synthase. Structure, 1996, 4, 801-810.	3.3	146
9	Crystal Structure of Exo-inulinase from Aspergillus awamori: The Enzyme Fold and Structural Determinants of Substrate Recognition. Journal of Molecular Biology, 2004, 344, 471-480.	4.2	141
10	Multi-scale structural and chemical analysis of sugarcane bagasse in the process of sequential acid–base pretreatment and ethanol production by Scheffersomyces shehatae and Saccharomyces cerevisiae. Biotechnology for Biofuels, 2014, 7, 63.	6.2	134
11	β-Lactoglobulin. International Dairy Journal, 1998, 8, 65-72.	3.0	129
12	The High Resolution Crystal Structure of Yeast Hexokinase PII with the Correct Primary Sequence Provides New Insights into Its Mechanism of Action. Journal of Biological Chemistry, 2000, 275, 20814-20821.	3.4	126
13	SAXSMoW 2.0: Online calculator of the molecular weight of proteins in dilute solution from experimental SAXS data measured on a relative scale. Protein Science, 2019, 28, 454-463.	7.6	122
14	Crystal Structure of Recombinant Human Interleukin-22. Structure, 2002, 10, 1051-1062.	3.3	119
15	Efficient sugar production from sugarcane bagasse by microwave assisted acid and alkali pretreatment. Biomass and Bioenergy, 2016, 93, 269-278.	5.7	115
16	Structural diversity of carbohydrate esterases. Biotechnology Research and Innovation, 2017, 1, 35-51.	0.9	114
17	The two types of 3-dehydroquinase have distinct structures but catalyze the same overall reaction. Nature Structural Biology, 1999, 6, 521-525.	9.7	113
18	Effects of pretreatment on morphology, chemical composition and enzymatic digestibility of eucalyptus bark: a potentially valuable source of fermentable sugars for biofuel production – part 1. Biotechnology for Biofuels, 2013, 6, 75.	6.2	108

#	Article	IF	CITATIONS
19	Structural Rearrangements in the Thyroid Hormone Receptor Hinge Domain and Their Putative Role in the Receptor Function. Journal of Molecular Biology, 2006, 360, 586-598.	4.2	106
20	Molecular Mechanism of Peroxisome Proliferator-Activated Receptor α Activation by WY14643: a New Mode of Ligand Recognition and Receptor Stabilization. Journal of Molecular Biology, 2013, 425, 2878-2893.	4.2	101
21	Involvement of the C terminus in intramolecular nitrogen channeling in glucosamine 6-phosphate synthase: evidence from a 1.6 å crystal structure of the isomerase domain. Structure, 1998, 6, 1047-1055.	3.3	99
22	Evaluating the composition and processing potential of novel sources of Brazilian biomass for sustainable biorenewables production. Biotechnology for Biofuels, 2014, 7, 10.	6.2	87
23	Structural Basis for Low Catalytic Activity in Lys49 Phospholipases A2A Hypothesis:  The Crystal Structure of Piratoxin II Complexed to Fatty Acid,. Biochemistry, 2001, 40, 28-36.	2.5	84
24	Mode of Peroxisome Proliferator-Activated Receptor Î ³ Activation by Luteolin. Molecular Pharmacology, 2012, 81, 788-799.	2.3	84
25	Structural and compositional changes in sugarcane bagasse subjected to hydrothermal and organosolv pretreatments and their impacts on enzymatic hydrolysis. Industrial Crops and Products, 2018, 113, 64-74.	5.2	84
26	Crystal Structures of β-Galactosidase from Penicillium sp. and its Complex with Galactose. Journal of Molecular Biology, 2004, 343, 1281-1292.	4.2	83
27	Dissecting structure–function–stability relationships of a thermostable GH5-CBM3 cellulase from <i>Bacillus subtilis</i> 168. Biochemical Journal, 2012, 441, 95-104.	3.7	81
28	Stability of l-asparaginase: an enzyme used in leukemia treatment. Pharmaceutica Acta Helvetiae, 1999, 74, 1-9.	1.2	79
29	Crystal structure of the ILâ€22/ILâ€22R1 complex and its implications for the ILâ€22 signaling mechanism. FEBS Letters, 2008, 582, 2985-2992.	2.8	76
30	Gaining ligand selectivity in thyroid hormone receptors via entropy. Proceedings of the National Academy of Sciences of the United States of America, 2009, 106, 20717-20722.	7.1	76
31	Carbohydrate binding modules enhance cellulose enzymatic hydrolysis by increasing access of cellulases to the substrate. Carbohydrate Polymers, 2019, 211, 57-68.	10.2	75
32	Molecular Dynamics Simulations of Ligand Dissociation from Thyroid Hormone Receptors:Â Evidence of the Likeliest Escape Pathway and Its Implications for the Design of Novel Ligands. Journal of Medicinal Chemistry, 2006, 49, 23-26.	6.4	73
33	Nuclear receptor full-length architectures: confronting myth and illusion with high resolution. Trends in Biochemical Sciences, 2015, 40, 16-24.	7.5	73
34	Quantitative 13C MultiCP solid-state NMR as a tool for evaluation of cellulose crystallinity index measured directly inside sugarcane biomass. Biotechnology for Biofuels, 2015, 8, 110.	6.2	72
35	Structural features of lignin obtained at different alkaline oxidation conditions from sugarcane bagasse. Industrial Crops and Products, 2012, 35, 61-69.	5.2	71
36	The MX2 macromolecular crystallography beamline: a wiggler X-ray source at the LNLS. Journal of Synchrotron Radiation, 2009, 16, 69-75.	2.4	70

#	Article	IF	CITATIONS
37	Crystal Structure of α-Galactosidase from Trichoderma reesei and Its Complex with Galactose: Implications for Catalytic Mechanism. Journal of Molecular Biology, 2004, 339, 413-422.	4.2	69
38	Molecular Dynamics Simulations Reveal Multiple Pathways of Ligand Dissociation from Thyroid Hormone Receptors. Biophysical Journal, 2005, 89, 2011-2023.	0.5	66
39	Purification, characterization, gene cloning and preliminary X-ray data of the exo-inulinase from Aspergillus awamori. Biochemical Journal, 2002, 362, 131-135.	3.7	65
40	Mechanisms of Peroxisome Proliferator Activated Receptor Î ³ Regulation by Non-steroidal Anti-inflammatory Drugs. Nuclear Receptor Signaling, 2015, 13, nrs.13004.	1.0	63
41	Set-up and Experimental Parameters of the Protein Crystallography Beamline at the Brazilian National Synchrotron Laboratory. Journal of Synchrotron Radiation, 1998, 5, 72-76.	2.4	62
42	Mapping the lignin distribution in pretreated sugarcane bagasse by confocal and fluorescence lifetime imaging microscopy. Biotechnology for Biofuels, 2013, 6, 43.	6.2	61
43	Aspergillus niger β-Glucosidase Has a Cellulase-like Tadpole Molecular Shape. Journal of Biological Chemistry, 2013, 288, 32991-33005.	3.4	60
44	Sugarcane waste as a valuable source of lipophilic molecules. Industrial Crops and Products, 2015, 76, 95-103.	5.2	59
45	Ajulemic Acid, a Synthetic Nonpsychoactive Cannabinoid Acid, Bound to the Ligand Binding Domain of the Human Peroxisome Proliferator-activated Receptor γ. Journal of Biological Chemistry, 2007, 282, 18625-18633.	3.4	58
46	Nutrient availability shapes the microbial community structure in sugarcane bagasse compost-derived consortia. Scientific Reports, 2016, 6, 38781.	3.3	56
47	Divergence in macromolecular assembly: X-ray crystallographic structure analysis of lumazine synthase from Brucella abortus11Edited by R. Huber. Journal of Molecular Biology, 2000, 297, 1031-1036.	4.2	55
48	Ligand Dissociation from Estrogen Receptor Is Mediated by Receptor Dimerization: Evidence from Molecular Dynamics Simulations. Molecular Endocrinology, 2008, 22, 1565-1578.	3.7	54
49	A review on bioprocessing of paddy straw to ethanol using simultaneous saccharification and fermentation. Process Biochemistry, 2019, 85, 125-134.	3.7	53
50	Crystal structure of neurotoxin Ts1 from Tityus serrulatus provides insights into the specificity and toxicity of scorpion toxins 1 1Edited by R. Huber. Journal of Molecular Biology, 1999, 290, 175-184.	4.2	52
51	Only Subtle Protein Conformational Adaptations Are Required for Ligand Binding to Thyroid Hormone Receptors: Simulations Using a Novel Multipoint Steered Molecular Dynamics Approach. Journal of Physical Chemistry B, 2008, 112, 10741-10751.	2.6	51
52	Crystal structure of a soluble decoy receptor ILâ€22BP bound to interleukinâ€22. FEBS Letters, 2009, 583, 1072-1077.	2.8	50
53	Energetic Contributions and Topographical Organization of Ligand Binding Residues of Tissue Factor. Biochemistry, 1995, 34, 6310-6315.	2.5	49
54	The protein crystallography beamline at LNLS, the Brazilian National Synchrotron Light Source. Nuclear Instruments and Methods in Physics Research, Section A: Accelerators, Spectrometers, Detectors and Associated Equipment, 1998, 405, 159-164.	1.6	49

#	Article	IF	CITATIONS
55	Crystal structure of the Kunitz (STI)-type inhibitor from Delonix regia seeds. Biochemical and Biophysical Research Communications, 2003, 312, 1303-1308.	2.1	49
56	An overview on progress, advances, and future outlook for biohydrogen production technology. International Journal of Hydrogen Energy, 2022, 47, 37264-37281.	7.1	48
57	Interleukin-22 Forms Dimers that are Recognized by Two Interleukin-22R1 Receptor Chains. Biophysical Journal, 2008, 94, 1754-1765.	0.5	46
58	Closed Conformation of the Active Site Loop of Rabbit Muscle Triosephosphate Isomerase in the Absence of Substrate: Evidence of Conformational Heterogeneity. Journal of Molecular Biology, 2003, 334, 1023-1041.	4.2	45
59	Structure and function of interleukin-22 and other members of the interleukin-10 family. Cellular and Molecular Life Sciences, 2010, 67, 2909-2935.	5.4	45
60	High-throughput cloning, expression and purification of glycoside hydrolases using Ligation-Independent Cloning (LIC). Protein Expression and Purification, 2014, 99, 35-42.	1.3	44
61	Defining functional diversity for lignocellulose degradation in a microbial community using multi-omics studies. Biotechnology for Biofuels, 2018, 11, 166.	6.2	44
62	Role of Halogen Bonds in Thyroid Hormone Receptor Selectivity: Pharmacophore-Based 3D-QSSR Studies. Journal of Chemical Information and Modeling, 2009, 49, 2606-2616.	5.4	43
63	Structural Insights into Human Peroxisome Proliferator Activated Receptor Delta (PPAR-Delta) Selective Ligand Binding. PLoS ONE, 2012, 7, e33643.	2.5	43
64	Joint <scp>X</scp> â€ray crystallographic and molecular dynamics study of cellobiohydrolase I from <i><scp>T</scp>richodermaÂharzianum</i> : deciphering the structural features of cellobiohydrolase catalytic activity. FEBS Journal, 2013, 280, 56-69.	4.7	43
65	Structural and chemical basis for enhanced affinity and potency for a large series of estrogen receptor ligands: 2D and 3D QSAR studies. Journal of Molecular Graphics and Modelling, 2007, 26, 434-442.	2.4	42
66	Structural basis of GC-1 selectivity for thyroid hormone receptor isoforms. BMC Structural Biology, 2008, 8, 8.	2.3	42
67	Novel Zn2+-binding Sites in Human Transthyretin. Journal of Biological Chemistry, 2010, 285, 31731-31741.	3.4	42
68	Crystal structure and statistical coupling analysis of highly glycosylated peroxidase from royal palm tree (Roystonea regia). Journal of Structural Biology, 2010, 169, 226-242.	2.8	41
69	Mapping the Intramolecular Vibrational Energy Flow in Proteins Reveals Functionally Important Residues. Journal of Physical Chemistry Letters, 2011, 2, 2073-2078.	4.6	41
70	Analysis of Agonist and Antagonist Effects on Thyroid Hormone Receptor Conformation by Hydrogen/Deuterium Exchange. Molecular Endocrinology, 2011, 25, 15-31.	3.7	41
71	Flavonoid interactions with human transthyretin: Combined structural and thermodynamic analysis. Journal of Structural Biology, 2012, 180, 143-153.	2.8	41
72	Transcriptome Profile of Trichoderma harzianum IOC-3844 Induced by Sugarcane Bagasse. PLoS ONE, 2014, 9, e88689.	2.5	41

#	Article	IF	CITATIONS
73	Structure-Based Approach for the Study of Estrogen Receptor Binding Affinity and Subtype Selectivity. Journal of Chemical Information and Modeling, 2008, 48, 2243-2253.	5.4	40
74	Amino acid sequence of piratoxin-II, a myotoxic Lys49 phospholipase A2 homologue from Bothrops pirajai venom. Biochimie, 2000, 82, 245-250.	2.6	39
75	Purification, characterization, gene cloning and preliminary X-ray data of the exo-inulinase from Aspergillus awamori. Biochemical Journal, 2002, 362, 131.	3.7	39
76	Structural comparison ofEscherichia coliL-asparaginase in two monoclinic space groups. Acta Crystallographica Section D: Biological Crystallography, 2003, 59, 416-422.	2.5	39
77	Conformational differences between the wild type and V30M mutant transthyretin modulate its binding to genistein: Implications to tetramer stability and ligand-binding. Journal of Structural Biology, 2010, 170, 522-531.	2.8	39
78	Potential of oleaginous yeast Trichosporon sp . , for conversion of sugarcane bagasse hydrolysate into biodiesel. Bioresource Technology, 2017, 242, 161-168.	9.6	39
79	Structural insights into β-glucosidase transglycosylation based on biochemical, structural and computational analysis of two GH1 enzymes from Trichoderma harzianum. New Biotechnology, 2018, 40, 218-227.	4.4	39
80	Structural Characterization of B and non-B Subtypes of HIV-Protease: Insights into the Natural Susceptibility to Drug Resistance Development. Journal of Molecular Biology, 2007, 369, 1029-1040.	4.2	38
81	Structural and biochemical characterization of a GH3 β-glucosidase from the probiotic bacteria Bifidobacterium adolescentis. Biochimie, 2018, 148, 107-115.	2.6	38
82	Protein crystal structure solution by fast incorporation of negatively and positively charged anomalous scatterers. Acta Crystallographica Section D: Biological Crystallography, 2001, 57, 996-1002.	2.5	37
83	Herbaspirillum seropedicae signal transduction protein PII is structurally similar to the enteric GlnK. FEBS Journal, 2002, 269, 3296-3303.	0.2	36
84	Dissection of a Human Septin:Â Definition and Characterization of Distinct Domains within Human SEPT4. Biochemistry, 2006, 45, 13918-13931.	2.5	36
85	Functional characterization of a lytic polysaccharide monooxygenase from the thermophilic fungus Myceliophthora thermophila. PLoS ONE, 2018, 13, e0202148.	2.5	36
86	Structural analysis ofTityus serrulatusTs1 neurotoxin at atomic resolution: insights into interactions with Na+channels. Acta Crystallographica Section D: Biological Crystallography, 2003, 59, 405-415.	2.5	35
87	Cellulose nanofibers production using a set of recombinant enzymes. Carbohydrate Polymers, 2021, 256, 117510.	10.2	35
88	Different binding and recognition modes of GL479, a dual agonist of Peroxisome Proliferator-Activated Receptor $\hat{I} \pm \hat{I}^3$. Journal of Structural Biology, 2015, 191, 332-340.	2.8	34
89	Identification of a New Hormone-Binding Site on the Surface of Thyroid Hormone Receptor. Molecular Endocrinology, 2014, 28, 534-545.	3.7	33
90	Crystal structures of bovine beta-lactoglobulin in the orthorhombic space group C2221 . Structural differences between genetic variants A and B and features of the Tanford transition. FEBS Journal, 2001, 268, 477-484.	0.2	33

#	Article	IF	CITATIONS
91	Cloning, heterologous expression and biochemical characterization of a non-specific endoglucanase family 12 from Aspergillus terreus NIH2624. Biochimica Et Biophysica Acta - Proteins and Proteomics, 2017, 1865, 395-403.	2.3	32
92	X-ray Structure and Molecular Dynamics Simulations of Endoglucanase 3 from Trichoderma harzianum: Structural Organization and Substrate Recognition by Endoglucanases That Lack Cellulose Binding Module. PLoS ONE, 2013, 8, e59069.	2.5	32
93	3D QSAR comparative molecular field analysis on nonsteroidal farnesoid X receptor activators. Journal of Molecular Graphics and Modelling, 2007, 25, 921-927.	2.4	31
94	Crystal structure of yeast hexokinase PI in complex with glucose: A classical "induced fit―example revised. Proteins: Structure, Function and Bioinformatics, 2008, 72, 731-740.	2.6	31
95	An alternative conformation of ERÎ ² bound to estradiol reveals H12 in a stable antagonist position. Scientific Reports, 2017, 7, 3509.	3.3	31
96	Pressure denaturation of Î ² -lactoglobulin. FEBS Journal, 2000, 267, 2235-2241.	0.2	30
97	Three-Dimensional Structure of the Fab from a Human IgM Cold Agglutinin. Journal of Immunology, 2000, 165, 6422-6428.	0.8	30
98	Revealing the insoluble metasecretome of lignocellulose-degrading microbial communities. Scientific Reports, 2017, 7, 2356.	3.3	30
99	Targeted metatranscriptomics of compost-derived consortia reveals a GH11 exerting an unusual exo-1,4-β-xylanase activity. Biotechnology for Biofuels, 2017, 10, 254.	6.2	30
100	Crystal structures of bovine β-lactoglobulin in the orthorhombic space group C2221. FEBS Journal, 2001, 268, 477-484.	0.2	29
101	Hemocyanin facilitates lignocellulose digestion by wood-boring marine crustaceans. Nature Communications, 2018, 9, 5125.	12.8	29
102	Recent advances in the enzymatic production and applications of xylooligosaccharides. World Journal of Microbiology and Biotechnology, 2021, 37, 169.	3.6	29
103	The X-ray structure of a recombinant major urinary protein at 1.75â€Ã resolution. A comparative study of X-ray and NMR-derived structures. Acta Crystallographica Section D: Biological Crystallography, 2001, 57, 1863-1869.	2.5	28
104	On the subtle tuneability of cellulose hydrogels: implications for binding of biomolecules demonstrated for CBM 1. Journal of Materials Chemistry B, 2017, 5, 3879-3887.	5.8	28
105	1 H NMR investigation of water accessibility in cellulose of pretreated sugarcane bagasse. Biotechnology for Biofuels, 2014, 7, 127.	6.2	28
106	Family 1 carbohydrate binding-modules enhance saccharification rates. AMB Express, 2014, 4, 36.	3.0	27
107	Thermal adaptation strategies of the extremophile bacterium Thermus filiformis based on multi-omics analysis. Extremophiles, 2017, 21, 775-788.	2.3	27
108	Nanoscale conformational ordering in polyanilines investigated by SAXS and AFM. Journal of Colloid and Interface Science, 2007, 316, 376-387.	9.4	26

#	Article	IF	CITATIONS
109	Thermodynamic characterization of the palm tree Roystonea regia peroxidase stability. Biochimie, 2008, 90, 1737-1749.	2.6	26
110	Molecular Basis of the Thermostability and Thermophilicity of Laminarinases: X-ray Structure of the Hyperthermostable Laminarinase from <i>Rhodothermus marinus</i> and Molecular Dynamics Simulations. Journal of Physical Chemistry B, 2011, 115, 7940-7949.	2.6	26
111	Structure-based identification of novel PPAR gamma ligands. Bioorganic and Medicinal Chemistry Letters, 2013, 23, 5795-5802.	2.2	26
112	Biochemical and structural insights into a thermostable cellobiohydrolase from <i>MyceliophthoraÂthermophila</i> . FEBS Journal, 2018, 285, 559-579.	4.7	26
113	Xyloglucan processing machinery in Xanthomonas pathogens and its role in the transcriptional activation of virulence factors. Nature Communications, 2021, 12, 4049.	12.8	26
114	Three-dimensional structure of an unusual Kunitz (STI) type trypsin inhibitor from Copaifera langsdorffii. Biochimie, 2004, 86, 167-172.	2.6	25
115	Identification of a novel ligand binding motif in the transthyretin channel. Bioorganic and Medicinal Chemistry, 2010, 18, 100-110.	3.0	25
116	Effect of pH and temperature on the global compactness, structure, and activity of cellobiohydrolase Cel7A from Trichoderma harzianum. European Biophysics Journal, 2012, 41, 89-98.	2.2	25
117	Recombinant Trichoderma harzianum endoglucanase I (Cel7B) is a highly acidic and promiscuous carbohydrate-active enzyme. Applied Microbiology and Biotechnology, 2015, 99, 9591-9604.	3.6	25
118	Molecular characterization of a family 5 glycoside hydrolase suggests an induced-fit enzymatic mechanism. Scientific Reports, 2016, 6, 23473.	3.3	25
119	Purification, and Biochemical and Biophysical Characterization of Cellobiohydrolase I from Trichoderma harzianum IOC 3844. Journal of Microbiology and Biotechnology, 2011, 21, 808-817.	2.1	25
120	The structure of the D49 phospholipase A2piratoxin III fromBothrops pirajaireveals unprecedented structural displacement of the calcium-binding loop: possible relationship to cooperative substrate binding. Acta Crystallographica Section D: Biological Crystallography, 2003, 59, 255-262.	2.5	24
121	Nuclear magnetic resonance investigation of water accessibility in cellulose of pretreated sugarcane bagasse. Biotechnology for Biofuels, 2014, 7, 127.	6.2	24
122	Design of an enzyme cocktail consisting of different fungal platforms for efficient hydrolysis of sugarcane bagasse: Optimization and synergism studies. Biotechnology Progress, 2016, 32, 1222-1229.	2.6	24
123	Characterization of a New Glyoxal Oxidase from the Thermophilic Fungus Myceliophthora thermophila M77: Hydrogen Peroxide Production Retained in 5-Hydroxymethylfurfural Oxidation. Catalysts, 2018, 8, 476.	3.5	24
124	Environments of the four tryptophans in the extracellular domain of human tissue factor: comparison of results from absorption and fluorescence difference spectra of tryptophan replacement mutants with the crystal structure of the wild-type protein. Biophysical Journal, 1995, 69, 20-29.	0.5	23
125	Enhanced hydrolysis of hydrothermally and autohydrolytically treated sugarcane bagasse and understanding the structural changes leading to improved saccharification. Biomass and Bioenergy, 2020, 139, 105639.	5.7	23
126	Low-Resolution Molecular Models Reveal the Oligomeric State of the PPAR and the Conformational Organization of Its Domains in Solution. PLoS ONE, 2012, 7, e31852.	2.5	23

#	Article	IF	CITATIONS
127	The Characterization of the Endoglucanase Cel12A from Gloeophyllum trabeum Reveals an Enzyme Highly Active on β-Glucan. PLoS ONE, 2014, 9, e108393.	2.5	22
128	Insights into the structure and function of fungal βâ€mannosidases from glycoside hydrolase familyÂ2 based on multiple crystal structures of the <i>TrichodermaÂharzianum</i> enzyme. FEBS Journal, 2014, 281, 4165-4178.	4.7	22
129	Crystal structure of β1→6â€galactosidase from <i>Bifidobacterium bifidum</i> S17: trimeric architecture, molecular determinants of the enzymatic activity and its inhibition by αâ€galactose. FEBS Journal, 2016, 283, 4097-4112.	4.7	22
130	Multifaceted characterization of sugarcane bagasse under different steam explosion severity conditions leading to distinct enzymatic hydrolysis yields. Industrial Crops and Products, 2019, 139, 111542.	5.2	22
131	Functional characterization and comparative analysis of two heterologous endoglucanases from diverging subfamilies of glycosyl hydrolase family 45. Enzyme and Microbial Technology, 2019, 120, 23-35.	3.2	22
132	Catalytic mechanism of inulinase from Arthrobacter sp. S37. Biochemical and Biophysical Research Communications, 2008, 371, 600-605.	2.1	21
133	Structural and thermodynamic analysis of thrombin:suramin interaction in solution and crystal phases. Biochimica Et Biophysica Acta - Proteins and Proteomics, 2009, 1794, 873-881.	2.3	21
134	Crystal structures of Leptospira interrogans FAD-containing ferredoxin-NADP+ reductase and its complex with NADP+. BMC Structural Biology, 2007, 7, 69.	2.3	20
135	Crystal structure analysis of peroxidase from the palm tree Chamaerops excelsa. Biochimie, 2015, 111, 58-69.	2.6	20
136	RXR Agonist Modulates TR: Corepressor Dissociation Upon 9-cis Retinoic Acid Treatment. Molecular Endocrinology, 2015, 29, 258-273.	3.7	20
137	Liquid ammonia pretreatment optimization for improved release of fermentable sugars from sugarcane bagasse. Journal of Cleaner Production, 2021, 281, 123922.	9.3	20
138	Structural Insights into the β-Mannosidase fromT. reeseiObtained by Synchrotron Small-Angle X-ray Solution Scattering Enhanced by X-ray Crystallographyâ€. Biochemistry, 2002, 41, 9370-9375.	2.5	19
139	2D QSAR studies on thyroid hormone receptor ligands. Bioorganic and Medicinal Chemistry, 2007, 15, 4609-4617.	3.0	19
140	Side by Side Comparison of Chemical Compounds Generated by Aqueous Pretreatments of Maize Stover, Miscanthus and Sugarcane Bagasse. Bioenergy Research, 2014, 7, 1466-1480.	3.9	19
141	Transformation of xylan into value-added biocommodities using Thermobacillus composti GH10 xylanase. Carbohydrate Polymers, 2020, 247, 116714.	10.2	19
142	Phasing on Rapidly Soaked Ions. Methods in Enzymology, 2003, 374, 120-137.	1.0	18
143	A Novel Carbohydrate-binding Module from Sugar Cane Soil Metagenome Featuring Unique Structural and Carbohydrate Affinity Properties. Journal of Biological Chemistry, 2016, 291, 23734-23743.	3.4	18
144	A simple enzymatic assay for the quantification of C1-specific cellulose oxidation by lytic polysaccharide monooxygenases. Biotechnology Letters, 2020, 42, 93-102.	2.2	18

#	Article	IF	CITATIONS
145	Essential Metabolic Routes as a Way to ESKAPE From Antibiotic Resistance. Frontiers in Public Health, 2020, 8, 26.	2.7	18
146	Low Resolution Structures of the Retinoid X Receptor DNA-binding and Ligand-binding Domains Revealed by Synchrotron X-ray Solution Scattering. Journal of Biological Chemistry, 2003, 278, 16030-16038.	3.4	17
147	Inhibition of Human Transthyretin Aggregation by Non-Steroidal Anti-Inflammatory Compounds: A Structural and Thermodynamic Analysis. International Journal of Molecular Sciences, 2013, 14, 5284-5311.	4.1	17
148	Low-Resolution Structure and Fluorescence Anisotropy Analysis of Protein Tyrosine Phosphatase Î Catalytic Domain. Biophysical Journal, 2007, 92, 4424-4432.	0.5	16
149	Ligand induced interaction of thyroid hormone receptor beta with its coregulators. Journal of Steroid Biochemistry and Molecular Biology, 2008, 112, 205-212.	2.5	16
150	Exploring oyster mushroom (<i>Pleurotus ostreatus</i>) substrate preparation by varying phase I composting time: changes in bacterial communities and physicochemical composition of biomass impacting mushroom yields. Journal of Applied Microbiology, 2019, 126, 931-944.	3.1	16
151	The Ultimate Wavelength for Protein Crystallography?. Acta Crystallographica Section D: Biological Crystallography, 1997, 53, 734-737.	2.5	15
152	X-ray Bragg Diffraction in a Strong Acoustic Field. Journal of Applied Crystallography, 1998, 31, 60-66.	4.5	15
153	Comparison of different crystal forms of 3-dehydroquinase fromSalmonella typhiand its implication for the enzyme activity. Acta Crystallographica Section D: Biological Crystallography, 2002, 58, 798-804.	2.5	15
154	Helix 12 Dynamics and Thyroid Hormone Receptor Activity: Experimental and Molecular Dynamics Studies of Ile280 Mutants. Journal of Molecular Biology, 2011, 412, 882-893.	4.2	15
155	Pre-treatment of sugarcane bagasse with a combination of sodium hydroxide and lime for improving the ruminal degradability: optimization of process parameters using response surface methodology. Journal of Applied Animal Research, 2016, 44, 287-296.	1.2	15
156	Cellulose ionics: switching ionic diode responses by surface charge in reconstituted cellulose films. Analyst, The, 2017, 142, 3707-3714.	3.5	15
157	Biochemical and biophysical characterization of novel GH10 xylanase prospected from a sugar cane bagasse compost-derived microbial consortia. International Journal of Biological Macromolecules, 2018, 109, 560-568.	7.5	15
158	Crystallization and preliminary X-ray diffraction studies of piratoxin III, a D-49 phospholipase A2 from the venom of Bothrops pirajai. Acta Crystallographica Section D: Biological Crystallography, 1999, 55, 1229-1230.	2.5	14
159	Substrate specificity of the Chamaerops excelsa palm tree peroxidase. A steady-state kinetic study. Journal of Molecular Catalysis B: Enzymatic, 2012, 74, 103-108.	1.8	14
160	A Novel Member of GH16 Family Derived from Sugarcane Soil Metagenome. Applied Biochemistry and Biotechnology, 2015, 177, 304-317.	2.9	14
161	Structure, computational and biochemical analysis of PcCel45A endoglucanase from Phanerochaete chrysosporium and catalytic mechanisms of GH45 subfamily C members. Scientific Reports, 2018, 8, 3678.	3.3	14
162	Physical techniques shed light on the differences in sugarcane bagasse structure subjected to steam explosion pretreatments at equivalent combined severity factors. Industrial Crops and Products, 2020, 158, 113003.	5.2	14

#	Article	IF	CITATIONS
163	Light-stimulated T. thermophilus two-domain LPMO9H: Low-resolution SAXS model and synergy with cellulases. Carbohydrate Polymers, 2021, 260, 117814.	10.2	14
164	Human Thyroid Receptor Forms Tetramers in Solution, Which Dissociate Into Dimers Upon Ligand Binding. Cell Biochemistry and Biophysics, 2006, 44, 453-462.	1.8	13
165	Low-Resolution Structures of Thyroid Hormone Receptor Dimers and Tetramers in Solutionâ€. Biochemistry, 2007, 46, 1273-1283.	2.5	13
166	Recognition by the Thyroid Hormone Receptor of Canonical DNA Response Elements. Biochemistry, 2010, 49, 893-904.	2.5	13
167	Functional characterization of a novel thermophilic exo-arabinanase from Thermothielavioides terrestris. Applied Microbiology and Biotechnology, 2020, 104, 8309-8326.	3.6	13
168	Comparative analysis of two recombinant LPMOs from Aspergillus fumigatus and their effects on sugarcane bagasse saccharification. Enzyme and Microbial Technology, 2021, 144, 109746.	3.2	13
169	Structural Insights into the β-Xylosidase fromTrichoderma reeseiObtained by Synchrotron Small-Angle X-ray Scattering and Circular Dichroism Spectroscopyâ€. Biochemistry, 2005, 44, 15578-15584.	2.5	12
170	Interleukinâ \in 22 and Its Crystal Structure. Vitamins and Hormones, 2006, 74, 77-103.	1.7	12
171	Structural modeling of high-affinity thyroid receptor–ligand complexes. European Biophysics Journal, 2010, 39, 1523-1536.	2.2	12
172	Functional Characterization and Low-Resolution Structure of an Endoglucanase Cel45A from the Filamentous Fungus Neurospora crassa OR74A: Thermostable Enzyme with High Activity Toward Lichenan and β-Glucan. Molecular Biotechnology, 2015, 57, 574-588.	2.4	12
173	Structure and dynamics of Trichoderma harzianum Cel7B suggest molecular architecture adaptations required for a wide spectrum of activities on plant cell wall polysaccharides. Biochimica Et Biophysica Acta - General Subjects, 2019, 1863, 1015-1026.	2.4	12
174	Enzymes for lignocellulosic biomass polysaccharideÂvalorization and production of nanomaterials. Current Opinion in Green and Sustainable Chemistry, 2020, 26, 100397.	5.9	12
175	Paludibacter propionicigenes GH10 xylanase as a tool for enzymatic xylooligosaccharides production from heteroxylans. Carbohydrate Polymers, 2022, 275, 118684.	10.2	12
176	Crystallization and Preliminary X-Ray Diffraction Analysis of the Lumazine Synthase fromBrucella abortus. Journal of Structural Biology, 1998, 123, 175-178.	2.8	11
177	Crystallization and preliminary X-ray diffraction studies of isoform α1 of the human thyroid hormone receptor ligand-binding domain. Acta Crystallographica Section D: Biological Crystallography, 2004, 60, 1867-1870.	2.5	11
178	Statistical Coupling Analysis of Aspartic Proteinases Based on Crystal Structures of the Trichoderma reesei Enzyme and Its Complex with Pepstatin A. Journal of Molecular Biology, 2008, 382, 763-778.	4.2	11
179	The binding of synthetic triiodo l-thyronine analogs to human transthyretin: Molecular basis of cooperative and non-cooperative ligand recognition. Journal of Structural Biology, 2011, 173, 323-332.	2.8	11
180	Sets of Covariant Residues Modulate the Activity and Thermal Stability of GH1 β-Glucosidases. PLoS ONE, 2014, 9, e96627.	2.5	11

#	Article	IF	CITATIONS
181	Non-productive adsorption of bacterial β-glucosidases on lignins is electrostatically modulated and depends on the presence of fibronection type III-like domain. Enzyme and Microbial Technology, 2016, 87-88, 1-8.	3.2	11
182	The stability and aggregation properties of the GTPase domain from human SEPT4. Biochimica Et Biophysica Acta - Proteins and Proteomics, 2008, 1784, 1720-1727.	2.3	10
183	Small-angle X-ray scattering and structural modeling of full-length: cellobiohydrolase I from Trichoderma harzianum. Cellulose, 2013, 20, 1573-1585.	4.9	10
184	Xanthomonas campestris expansin-like X domain is a structurally disordered beta-sheet macromolecule capable of synergistically enhancing enzymatic efficiency of cellulose hydrolysis. Biotechnology Letters, 2015, 37, 2419-2426.	2.2	10
185	Biophysical and biochemical studies of a major endoglucanase secreted by Xanthomonas campestris pv. campestris Enzyme and Microbial Technology, 2016, 91, 1-7.	3.2	10
186	Cellulose fiber size defines efficiency of enzymatic hydrolysis and impacts degree of synergy between endo- and exoglucanases. Cellulose, 2018, 25, 1865-1881.	4.9	10
187	Low-resolution envelope, biophysical analysis and biochemical characterization of a short-chain specific and halotolerant carboxylesterase from Bacillus licheniformis. International Journal of Biological Macromolecules, 2018, 120, 1893-1905.	7.5	10
188	GH43 endo-arabinanase from Bacillus licheniformis: Structure, activity and unexpected synergistic effect on cellulose enzymatic hydrolysis. International Journal of Biological Macromolecules, 2018, 117, 7-16.	7.5	10
189	Enzymatic versatility and thermostability of a new aryl-alcohol oxidase from Thermothelomyces thermophilus M77. Biochimica Et Biophysica Acta - General Subjects, 2020, 1864, 129681.	2.4	10
190	Evaluating the Potential of Culms from Sugarcane and Energy Cane Varieties Grown in Argentina for Second-Generation Ethanol Production. Waste and Biomass Valorization, 2022, 13, 329-343.	3.4	10
191	Two- and Three-Dimensional Quantitative Structure-Activity Relationships Studies on a Series of Liver X Receptor Ligands. Open Medicinal Chemistry Journal, 2008, 2, 87-96.	2.4	10
192	Determination of crystal imperfection by X-ray diffraction in a strong acoustic field. Journal of Applied Crystallography, 1992, 25, 88-91.	4.5	9
193	Visualization of acoustic fields in surface acoustic wave devices by means of X-ray topography. Nuclear Instruments & Methods in Physics Research B, 1995, 97, 346-350.	1.4	9
194	Effect of absorption on dynamical Bragg diffraction of x-rays on a crystal modulated by strong ultrasound. Journal Physics D: Applied Physics, 1997, 30, 2591-2595.	2.8	9
195	Quantitative structure-activity relationships for a series of selective estrogen receptor-beta modulators. SAR and QSAR in Environmental Research, 2007, 18, 711-727.	2.2	9
196	Crystallization and preliminary X-ray crystallographic analysis of the heterodimeric crotoxin complex and the isolated subunits crotapotin and phospholipase A2. Acta Crystallographica Section F: Structural Biology Communications, 2007, 63, 287-290.	0.7	9
197	Dissecting the Relation between a Nuclear Receptor and GATA: Binding Affinity Studies of Thyroid Hormone Receptor and GATA2 on TSHÎ ² Promoter. PLoS ONE, 2010, 5, e12628.	2.5	9
198	Combination of Sodium Hydroxide and Lime as a Pretreatment for Conversion of Date Palm Leaves into a Promising Ruminant Feed: An Optimization Approach. Waste and Biomass Valorization, 2015, 6, 243-252.	3.4	9

#	Article	IF	CITATIONS
199	Biochemical characterization and low-resolution SAXS shape of a novel GH11 exo-1,4-β-xylanase identified in a microbial consortium. Applied Microbiology and Biotechnology, 2019, 103, 8035-8049.	3.6	9
200	Polymer ultrastructure governs AA9 lytic polysaccharide monooxygenases functionalization and deconstruction efficacy on cellulose nano-crystals. Bioresource Technology, 2022, 347, 126375.	9.6	9
201	Purification, crystallization and preliminary X-ray study of β-xylosidase fromTrichoderma reesei. Acta Crystallographica Section D: Biological Crystallography, 2000, 56, 1058-1060.	2.5	8
202	Hologram QSAR Studies on Farnesoid X Receptor Activators. Letters in Drug Design and Discovery, 2006, 3, 261-267.	0.7	8
203	Doping in poly(o-ethoxyaniline) nanostructured films studied with atomic force spectroscopy (AFS). Micron, 2008, 39, 1119-1125.	2.2	8
204	On the Denaturation Mechanisms of the Ligand Binding Domain of Thyroid Hormone Receptors. Journal of Physical Chemistry B, 2010, 114, 1529-1540.	2.6	8
205	Enzymes in Bioenergy. , 2011, , 97-113.		8
206	A novel thermostable GH5 β-xylosidase from Thermogemmatispora sp. T81. New Biotechnology, 2019, 53, 57-64.	4.4	8
207	Biochemical characterization and low-resolution SAXS structure of two-domain endoglucanase BICel9 from Bacillus licheniformis. Applied Microbiology and Biotechnology, 2019, 103, 1275-1287.	3.6	8
208	Structural and molecular dynamics investigations of ligand stabilization via secondary binding site interactions in Paenibacillus xylanivorans GH11 xylanase. Computational and Structural Biotechnology Journal, 2021, 19, 1557-1566.	4.1	8
209	Crystallization and synchrotron X-ray diffraction studies of human interleukin-22. Acta Crystallographica Section D: Biological Crystallography, 2002, 58, 529-530.	2.5	7
210	Expression, purification, and characterization of rat protein tyrosine phosphatase η catalytic domain. Protein Expression and Purification, 2005, 41, 113-120.	1.3	7
211	Effectiveness of commercial inhibitors against subtype F HIV-1 protease. Journal of Enzyme Inhibition and Medicinal Chemistry, 2009, 24, 638-645.	5.2	7
212	Purification, crystallization and preliminary crystallographic analysis of the catalytic domain of the extracellular cellulase CBHI fromTrichoderma harzianum. Acta Crystallographica Section F: Structural Biology Communications, 2010, 66, 1041-1044.	0.7	7
213	Isolation and characterization of a β-galactosidase from a new Amazon forest strain of <i>Aspergillus niger</i> as a potential accessory enzyme for biomass conversion. Biocatalysis and Biotransformation, 2014, 32, 13-22.	2.0	7
214	The effect of lime pre-treatments of date palm leaves on delignification and <i>in vitro</i> rumen degradability. Journal of Agricultural Science, 2017, 155, 184-190.	1.3	7
215	Ionic Diodes Based on Regenerated αâ€Cellulose Films Deposited Asymmetrically onto a Microhole. ChemistrySelect, 2017, 2, 871-875.	1.5	7
216	Crystal structure of a small heat-shock protein from <i>Xylella fastidiosa</i> reveals a distinct high-order structure. Acta Crystallographica Section F, Structural Biology Communications, 2017, 73, 222-227.	0.8	7

#	Article	IF	CITATIONS
217	Insights into the dual cleavage activity of the GH16 laminarinase enzyme class on β-1,3 and β-1,4 glycosidic bonds. Journal of Biological Chemistry, 2021, 296, 100385.	3.4	7
218	On the Choice of an Optimal Wavelength in Macromolecular Crystallography. Acta Crystallographica Section D: Biological Crystallography, 1998, 54, 610-614.	2.5	6
219	Crystallization and preliminary X-ray diffraction studies of human catalase. Acta Crystallographica Section D: Biological Crystallography, 1999, 55, 1614-1615.	2.5	6
220	Purification, crystallization and preliminary diffraction study of β-galactosidase fromPenicilliumÂsp Acta Crystallographica Section D: Biological Crystallography, 2000, 56, 1508-1509.	2.5	6
221	Crystallization and preliminary X-ray diffraction analysis of a novel trypsin inhibitor from seeds ofCopaifera langsdorffii. Acta Crystallographica Section D: Biological Crystallography, 2001, 57, 1316-1318.	2.5	6
222	Getting the most out of X-ray home sources. Acta Crystallographica Section D: Biological Crystallography, 2005, 61, 1022-1030.	2.5	6
223	Structural Analysis of an Echinococcus granulosus Actin-Fragmenting Protein by Small-Angle X-Ray Scattering Studies and Molecular Modeling. Biophysical Journal, 2006, 90, 3216-3223.	0.5	6
224	Purification, crystallization and preliminary X-ray diffraction analysis of royal palm tree (Roystonea) Tj ETQq0 0 0 780-783.	rgBT /Ove 0.7	rlock 10 Tf 50 6
225	Orphan nuclear receptor NGFI-B forms dimers with nonclassical interface. Protein Science, 2007, 16, 1762-1772.	7.6	6
226	Fluorescence spectroscopy as a tool to detect and evaluate glucocorticoid-induced skin atrophy. Lasers in Medical Science, 2012, 27, 1059-1065.	2.1	6
227	Crystallization and preliminary X-ray diffraction analysis of endoglucanase III fromTrichoderma harzianum. Acta Crystallographica Section F: Structural Biology Communications, 2012, 68, 306-309.	0.7	6
228	Expression, purification, crystallization and preliminary X-ray diffraction analysis of <i>Aspergillus terreus</i> endo-β-1,4-glucanase from glycoside hydrolase family 12. Acta Crystallographica Section F, Structural Biology Communications, 2014, 70, 267-270.	0.8	6
229	HTP-OligoDesigner: An Online Primer Design Tool for High-Throughput Gene Cloning and Site-Directed Mutagenesis. Journal of Computational Biology, 2016, 23, 27-29.	1.6	6
230	Production of prebiotic xylooligosaccharides from arabino- and glucuronoxylan using a two-domain Jonesia denitrificans xylanase from GH10 family. Enzyme and Microbial Technology, 2021, 144, 109743.	3.2	6
231	Impact of cellulose properties on enzymatic degradation by bacterial GH48 enzymes: Structural and mechanistic insights from processive Bacillus licheniformis Cel48B cellulase. Carbohydrate Polymers, 2021, 264, 118059.	10.2	6
232	Acoustically adjustable LiNbO3 double-crystal monochromator for synchrotron radiation. Review of Scientific Instruments, 1999, 70, 2230-2234.	1.3	5
233	Purification, crystallization and preliminary crystallographic study of a Kunitz-type trypsin inhibitor from Delonix regia seeds. Acta Crystallographica Section D: Biological Crystallography, 1999, 55, 1611-1613.	2.5	5
234	Crystallization and preliminary X-ray diffraction analysis of the catalytic subunit of ADP–glucose pyrophosphorylase from potato tuber. Acta Crystallographica Section D: Biological Crystallography, 2000, 56, 192-194.	2.5	5

#	Article	IF	CITATIONS
235	Crystallization of a non-B and a B mutant HIV protease. Acta Crystallographica Section D: Biological Crystallography, 2004, 60, 1625-1627.	2.5	5
236	Camptosemin, a tetrameric lectin of Camptosema ellipticum: structural and functional analysis. European Biophysics Journal, 2010, 39, 1193-1205.	2.2	5
237	Biochemical characterization and low-resolution SAXS structure of an exo-polygalacturonase from Bacillus licheniformis. New Biotechnology, 2018, 40, 268-274.	4.4	5
238	Analysis of carbohydrate-active enzymes in <i>Thermogemmatispora</i> sp. strain T81 reveals carbohydrate degradation ability. Canadian Journal of Microbiology, 2018, 64, 992-1003.	1.7	5
239	Crystallographic structure and molecular dynamics simulations of the major endoglucanase from Xanthomonas campestris pv. campestris shed light on its oligosaccharide products release pattern. International Journal of Biological Macromolecules, 2019, 136, 493-502.	7.5	5
240	X-ray Structure, Bioinformatics Analysis, and Substrate Specificity of a 6-Phospho-Î ² -glucosidase Glycoside Hydrolase 1 Enzyme from <i>Bacillus licheniformis</i> . Journal of Chemical Information and Modeling, 2020, 60, 6392-6407.	5.4	5
241	Unlocking the structural features for the xylobiohydrolase activity of an unusual GH11 member identified in a compostâ€derived consortium. Biotechnology and Bioengineering, 2021, 118, 4052-4064.	3.3	5
242	SAXSMoW 3.0: New advances in the determination of the molecular weight of proteins in dilute solutions from SAXS intensity data on a relative scale. Protein Science, 2021, , .	7.6	5
243	Protein Crystallography in the Soft X-ray Region: Crystal Lifetime and Diffraction Efficiency. Journal of Synchrotron Radiation, 1997, 4, 17-20.	2.4	4
244	Double-crystal diffractive modulator of synchrotron radiation. Review of Scientific Instruments, 1998, 69, 2218-2222.	1.3	4
245	Crystallization and preliminary X-ray analysis of bucain, a novel toxin from the Malayan kraitBungarus candidus. Acta Crystallographica Section D: Biological Crystallography, 2002, 58, 1879-1881.	2.5	4
246	SAXS Studies of the Endoglucanase Cel12A from Gloeophyllum trabeum Show Its Monomeric Structure and Reveal the Influence of Temperature on the Structural Stability of the Enzyme. Materials, 2014, 7, 5202-5211.	2.9	4
247	Structural and biochemical data of Trichoderma harzianum GH1 β-glucosidases. Data in Brief, 2017, 15, 340-343.	1.0	4
248	Biochemical characterization, low-resolution SAXS structure and an enzymatic cleavage pattern of BICel48 from Bacillus licheniformis. International Journal of Biological Macromolecules, 2018, 111, 302-310.	7.5	4
249	Multienzyme Cellulose Films as Sustainable and Self-Degradable Hydrogen Peroxide-Producing Material. Biomacromolecules, 2020, 21, 5315-5322.	5.4	4
250	A linker of the proline-threonine repeating motif sequence is bimodal. Journal of Molecular Modeling, 2020, 26, 178.	1.8	4
251	When the order matters: Impacts of lignin removal and xylan conformation on the physical structure and enzymatic hydrolysis of sugarcane bagasse. Industrial Crops and Products, 2022, 180, 114708.	5.2	4
252	X-ray diffraction in crystals in the presence of laser-induced dynamic gratings. Journal Physics D: Applied Physics, 1996, 29, 2148-2155.	2.8	3

#	Article	IF	CITATIONS
253	Preliminary X-ray diffraction studies of rabbit muscle triose phosphate isomerase (TIM). Acta Crystallographica Section D: Biological Crystallography, 2000, 56, 1492-1494.	2.5	3
254	Expression, purification, and initial structural characterization of rat orphan nuclear receptor NOR-1 LBD domain. Protein Expression and Purification, 2004, 37, 443-449.	1.3	3
255	Crystallization and preliminary X-ray diffraction studies of ferredoxin reductase fromLeptospira interrogans. Acta Crystallographica Section F: Structural Biology Communications, 2006, 62, 662-664.	0.7	3
256	Differential effects of TR ligands on hormone dissociation rates: Evidence for multiple ligand entry/exit pathways. Journal of Steroid Biochemistry and Molecular Biology, 2009, 117, 125-131.	2.5	3
257	Nanostructured Sensors Containing Immobilized Nuclear Receptors for Thyroid Hormone Detection. Journal of Biomedical Nanotechnology, 2014, 10, 744-750.	1.1	3
258	Draft Genome Sequence of the Thermophile Thermus filiformis ATCC 43280, Producer of Carotenoid-(Di)glucoside-Branched Fatty Acid (Di)esters and Source of Hyperthermostable Enzymes of Biotechnological Interest. Genome Announcements, 2015, 3, .	0.8	3
259	Crystal structure of a putative exo-l²-1,3-galactanase from <i>Bifidobacterium bifidum</i> S17. Acta Crystallographica Section F, Structural Biology Communications, 2016, 72, 288-293.	0.8	3
260	Biochemical Characterization and Low-Resolution SAXS Molecular Envelope of GH1 β-Glycosidase from Saccharophagus degradans. Molecular Biotechnology, 2016, 58, 777-788.	2.4	3
261	Structural insights into the hydrolysis pattern and molecular dynamics simulations of CH45 subfamily a endoglucanase from Neurospora crassa OR74A. Biochimie, 2019, 165, 275-284.	2.6	3
262	Differences in chemical composition and physical properties caused by industrial storage on sugarcane bagasse result in its efficient enzymatic hydrolysis. Sustainable Energy and Fuels, 2022, 6, 329-348.	4.9	3
263	Optimization of Dilute Acid Pretreatment for Enhanced Release of Fermentable Sugars from Sugarcane Bagasse and Validation by Biophysical Characterization. Bioenergy Research, 2023, 16, 416-434.	3.9	3
264	Crystallization and preliminary diffraction data of neurotoxin Ts-γ from the venom of the scorpion Tityus serrulatus. Acta Crystallographica Section D: Biological Crystallography, 1998, 54, 1440-1441.	2.5	2
265	Adjustable x-ray phase plate and phase modulator. Applied Physics Letters, 1998, 73, 2096-2097.	3.3	2
266	Crystallization and preliminary crystal analysis of yeast hexokinase PI and PII. Acta Crystallographica Section D: Biological Crystallography, 1999, 55, 2047-2048.	2.5	2
267	Probing conformational changes in orphan nuclear receptor: The NGFI-B intermediate is a partially unfolded dimer. Biophysical Chemistry, 2008, 137, 81-87.	2.8	2
268	Purification, crystallization and preliminary crystallographic analysis of peroxidase from the palm tree <i>Chamaerops excelsa</i> . Acta Crystallographica Section F: Structural Biology Communications, 2011, 67, 1641-1644.	0.7	2
269	Crystallization and preliminary diffraction analysis of the catalytic domain of major extracellular endoglucanase fromXanthomonas campestrispv.campestris. Acta Crystallographica Section F: Structural Biology Communications, 2013, 69, 137-140.	0.7	2
270	Cloning, purification, crystallization and preliminary X-ray studies of a carbohydrate-binding module (CBM_E1) derived from sugarcane soil metagenome. Acta Crystallographica Section F, Structural Biology Communications, 2014, 70, 1232-1235.	0.8	2

#	Article	IF	CITATIONS
271	Short communication: investigating the effect of saffron (Crocus sativus L.) nano-sizing on its colour extraction efficiency: a preliminary study. Natural Product Research, 2017, 31, 2308-2311.	1.8	2
272	Differences in Gluco and Galacto Substrate-Binding Interactions in a Dual 6Pβ-Glucosidase/6Pβ-Galactosidase Glycoside Hydrolase 1 Enzyme from <i>Bacillus licheniformis</i> . Journal of Chemical Information and Modeling, 2021, 61, 4554-4570.	5.4	2
273	Characterization of Pretreated Fractions and Cellulosic Ethanol Production from Steam-Exploded <i>Eucalyptus urograndis</i> . Energy & Fuels, 2020, 34, 535-545.	5.1	2
274	A GH115 α-glucuronidase structure reveals dimerization-mediated substrate binding and a proton wire potentially important for catalysis. Acta Crystallographica Section D: Structural Biology, 2022, 78, 658-668.	2.3	2
275	Crystallization and preliminary X-ray diffraction studies of piratoxin II, a phospholipase A2 isolated from the venom of Bothrops pirajai. Acta Crystallographica Section D: Biological Crystallography, 1998, 54, 1437-1439.	2.5	1
276	Ultrasound adjustable Laue-Laue double-crystal x-ray monochromator. Journal Physics D: Applied Physics, 1999, 32, 2083-2086.	2.8	1
277	Preparation and preliminary X-ray diffraction studies of a new crystal form of L-asparaginase from Escherichia coli. Acta Crystallographica Section D: Biological Crystallography, 1999, 55, 1616-1617.	2.5	1
278	Crystallization and preliminary X-ray study of β-mannosidase fromTrichoderma reesei. Acta Crystallographica Section D: Biological Crystallography, 2000, 56, 342-343.	2.5	1
279	Crystallization and preliminary X-ray study of haem-binding protein from the bloodsucking insectRhodnius prolixus. Acta Crystallographica Section D: Biological Crystallography, 2001, 57, 860-861.	2.5	1
280	Crystallization and Preliminary Crystallographic Analysis of Laminarinase from Rhodothermus marinus: A Case of Pseudomerohedral Twinning. Protein and Peptide Letters, 2008, 15, 1142-1144.	0.9	1
281	Crystallization and preliminary X-ray diffraction analysis of human IL-22 bound to its soluble decoy receptor IL-22BP. Acta Crystallographica Section F: Structural Biology Communications, 2009, 65, 102-104.	0.7	1
282	Expression, purification, crystallization and preliminary X-ray diffraction analysis of the pectin methylesterase from the sugar cane weevilSphenophorus levis. Acta Crystallographica Section F, Structural Biology Communications, 2014, 70, 331-334.	0.8	1
283	Cloning, purification, crystallization and preliminary X-ray studies of a carbohydrate-binding module from family 64 (StX). Acta Crystallographica Section F, Structural Biology Communications, 2015, 71, 311-314.	0.8	1
284	Response to Moras et al Trends in Biochemical Sciences, 2015, 40, 290-292.	7.5	1
285	Structural dataset for the PPARÎ ³ V290M mutant. Data in Brief, 2016, 7, 1430-1437.	1.0	1
286	The structure of the extended E2 DNAâ€binding domain of the bovine papillomavirusâ€1. Proteins: Structure, Function and Bioinformatics, 2020, 88, 106-112.	2.6	1
287	Low-resolution molecular shape, biochemical characterization and emulsification properties of a halotolerant esterase from Bacillus licheniformis. European Biophysics Journal, 2020, 49, 435-447.	2.2	1
288	Evaluating the Composition and Processing Potential of Novel Sources of Brazilian Biomass for		1

Sustainable Biorenewables Production. , 2015, , 21-63.

#	Article	IF	CITATIONS
289	Crystallization and X-Ray Data Analysis of the Extended Dna-Binding Domain of the E2 Bovine Papillomavirus Type 1 Protein. Protein and Peptide Letters, 2001, 8, 323-326.	0.9	1
290	Resonance time Modulation of X-ray Diffraction in Crystals Deformed by Ultrasound. Journal of Applied Crystallography, 1998, 31, 388-391.	4.5	0
291	Crystallization and preliminary diffraction studies of a recombinant major urinary protein. Acta Crystallographica Section D: Biological Crystallography, 1999, 55, 1340-1341.	2.5	0
292	Crystallization and preliminary X-ray diffraction analysis of rat protein tyrosine phosphatase η. Acta Crystallographica Section F: Structural Biology Communications, 2006, 62, 923-925.	0.7	0
293	Development and validation of a fast RP-HPLC method to determine the analogue of the thyroid hormone, 3,5,3′-triiodothyroacetic acid (TRIAC), in polymeric nanoparticles. Analytical Methods, 2011, 3, 1936.	2.7	0
294	Expression, purification, crystallization and preliminary X-ray diffraction analysis ofBifidobacterium adolescentisxylose isomerase. Acta Crystallographica Section F: Structural Biology Communications, 2013, 69, 588-591.	0.7	0
295	Crystallization and preliminary X-ray diffraction analysis of a new xyloglucanase fromXanthomonas campestrispv.campestris. Acta Crystallographica Section F: Structural Biology Communications, 2013, 69, 676-678.	0.7	0
296	Effects of 3,5,3′-Triiodothyroacetic Acid, Nanoencapsulated or Not, on Intact and Atrophic Skin in Rats. Journal of Nanotechnology in Engineering and Medicine, 2014, 5, .	0.8	0
297	Conformational variability of the stationary phase survival protein E from <i>Xylella fastidiosa</i> revealed by X-ray crystallography, small-angle X-ray scattering studies, and normal mode analysis. Proteins: Structure, Function and Bioinformatics, 2017, 85, 1931-1943.	2.6	0
298	Crystal Structure of Limonoid 6- <i>O</i> -Acetylswietephragmin <i>E</i> and Theoretical Study of Nuclear Magnetic Resonance Spectra of Phragmalin Limonoids. Advanced Science Letters, 2012, 18, 150-157.	0.2	0
299	Biomassa lignocelulósica: estrutura e composição. , 2020, , 9-30.		Ο